Probing the emission region using anomalous lensed QSO's

David Floyd[1,2,3], Nick Bate[1], Rachel Webster[1]

email: dfloyd@lco.cl

In gravitational lensing theory, it is predicted that two images which straddle a caustic will have the same magnification. However there are a significant number of well-observed cases where a factor of up to 10 is observed in the magnification ratio - **"anomalous lensed quasars"**. These offer a unique window on the nature of both lens and lensed source: From recent modelling (B+07, C+07) it appears that the size of the emission region convolved with the microlensing pattern is the main reason for the discrepancy. With appropriate modelling, this can be turned around, and a measurement of the emission region of the quasar can be made. This is particularly interesting if a range of observations are made, either at different times (to more highly constrain the probability distribution) or in different wavebands (to constrain the size as a function of λ). We present recent multi-band observations of **MG0414+0534** as a case study, demonstrating that the anomalous A2/A1 flux ratio decreases as we move blueward, and use the results to **constrain the size of the r-band AGN emission region to < 7 light days.**

Background

Macrolensing

Images are formed at the positions where the optical path length is stationary - minima, maxima and saddle points of the Fermat travel-time surface (Fermat's principle). Magnification μ is determined by convergence κ_{tot} and the shear γ of the lens at the image locations:

$$\mu = \frac{1}{[(1-\kappa_{tot})+\gamma][(1-\kappa_{tot})-\gamma]}$$

Maxima and saddles may exhibit demagnification, while **minima are always magnified**. In a quadruple system, the brightest image pair are found at a saddle point and a minimum. Images are magnified by a factor of ~5-20.

Microlensing

As discussed in SW02, the convergence κ can be split into two components: smooth (κ_s), and compact (κ_*). Introducing small-scale perturbations in the lens potential (microlensing) produces new features in the Fermat surface - **see figure 1**. The simple case of one microlens is familiar from planetary transits. In the macrolens case, each macro-saddle or macro-minimum contains a large number of micro-saddle points (one for each star in the lens). This has been found to explain the anomalous fluxes seen in some quasars (WMS95). Dust (L+95) and millilensing by galactic substructure (MS98, MM01, C02, DK02) have also been explored as possible causes. However, millilensing should also affect the radio emission, for which an anomalous flux ratio is not observed.

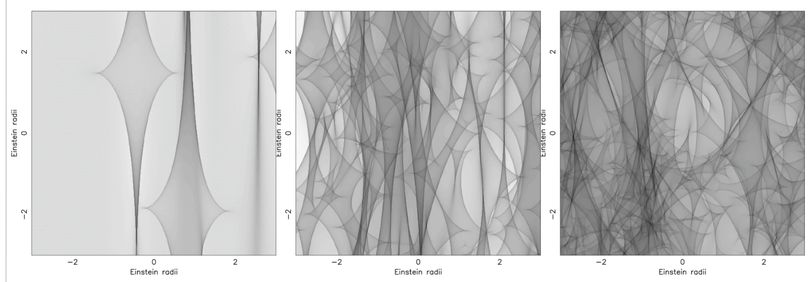

Fig. 1: Magnification maps showing the magnification with position for a simulation. Darker areas correspond to regions of higher magnification. From left-to-right we have a clumpy matter content of 1%, 30% and 100%. The uncrowded 1% figure at left should be familiar from planetary transit studies. Increased microlensing due to the clumps produces a complicated Fermat travel-time surface and thus magnification map. Anomalous lensed quasars occur when the saddlepoint image is only weakly magnified, but the min image magnified.

Objective

Lensed quasars have been used before to place upper limits on the size of the emission region - most notably in Q2237+0305 (WMS95, W+05). Furthermore, it has been shown that changing the content of the lens can produce anomalous flux ratios (SW02). **However, combining these two effects was only recently attempted (Bate et al. 2007). Our new objective is to explore source size with wavelength.**

Observations & Fitting

We began observations on the Magellan telescopes in Nov. 2007. The aim is to get multi-band imaging of anomalous lensed QSO's in a single night using PANIC and IMACS. We use bright nights with excellent seeing. Integration times are ~5 minutes per filter, (10 mins in the blue). There are 6 known anomalous quasars accessible from the south of which we have observed 3. We fit astigmatism (A) and defocus (D) to the entire 30 arcmin IMACS field of view and produce a modified Gaussian ("Waussian") PSF for the positions of the quasar images with an ellipticity and angle prescribed by the (A,D) pattern found (Floyd & Schechter in preparation). We use direct fitting of this PSF to each quasar image. We are experimenting with deconvolution techniques, using pre-existing HST images as models.

MG0414+0534

Observed 2007/11/03 in 0".5 seeing. See **Fig. 2**. This is our first test case, and A1 and A2 are only just resolved. However, it is clear that the A2/A1 ratio becomes more anomalous as we move blueward. In g, A2 is undetected.

SDSS0924+0219

Observed on 2008/05/21 in 0".35 seeing. A1 and A2 clearly resolved, but A2 very faint.

WFI2026-4536

Observed on 2008/05/21 in 0".35 seeing. A1 and A2 are just resolved.

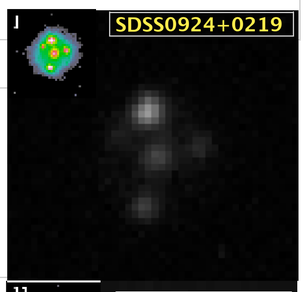

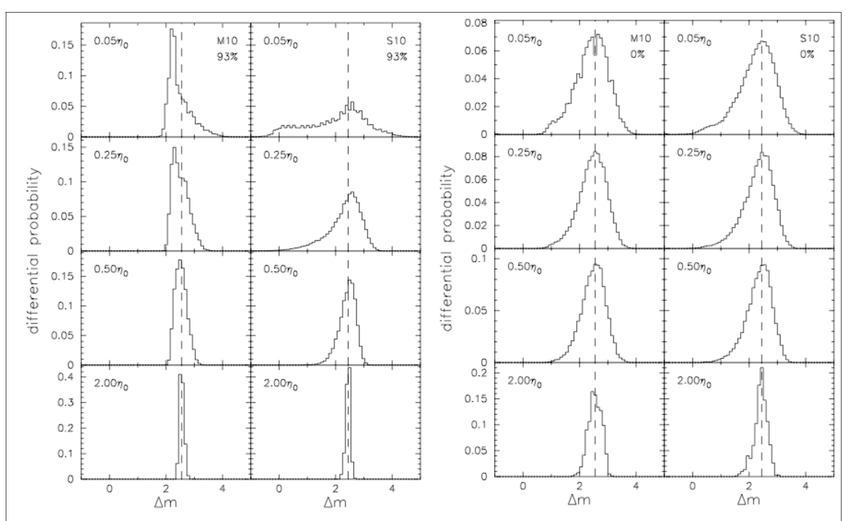

Fig. 3: Differential probability histograms for magnification in case of 93% smooth matter (left) and 0% smooth matter (right). Left and right columns correspond to the "minimum" and "saddle-point" macro-models, respectively (both with μ=10). Source size (in Einstein radii, η_0) increases as we move down. Anomalous fluxes demand a nonzero probability of low magnification in the saddlepoint image.

Simulations & Preliminary Results

Simulations

Microlensing simulations are conducted using a ray-shooting method (K+86; W+90). We allowed the smooth matter fraction in the lens to vary from 0 to 99% (see **Bate et al. (2007)** for full details). The model for MG0414+0534 is based on earlier work by SW02. **Fig. 3** illustrates the effect of source size and lens model on the magnification probability distribution: Increasing the smoothness of the lens increases the relative probability of a low-magnification saddle point image (right columns in Fig. 3) and thus of an anomalous flux ratio. Increasing source size completely eliminates the flat low-magnification wing, making anomalous fluxes impossible.

Results

We have obtained imaging of sufficient quality on 2 nights (2007/11/03 and 2008/05/21) to detect both members of an anomalous image pair. Data for MG0414+0534 has been modelled - see table 2: **It is clear that the A2/A1 ratio gets more anomalous as we get bluer, consistent with a decreasing source size.** We fit the emitting region with a power law, $R = R_0 \left(\frac{\lambda}{\lambda_o}\right)^{\gamma}$

Figure 4 shows our combined probability distribution for the optical data (r, i, z) and optical-IR (r, i, z, J) for MG0414+0534.

Band	A2/A1	Obs. date
g'	<0.20	2007/11/03 - unable to detect A2!
r'	0.21±0.1	2007/11/03
i'	0.26±0.1	2007/11/03
z'	0.34±0.1	2007/11/03
J	0.80±0.2	2007/11/03
H	0.85±0.2	2007/11/03

Table 1: Measurements of A_2/A_1 for MG0414+0534.

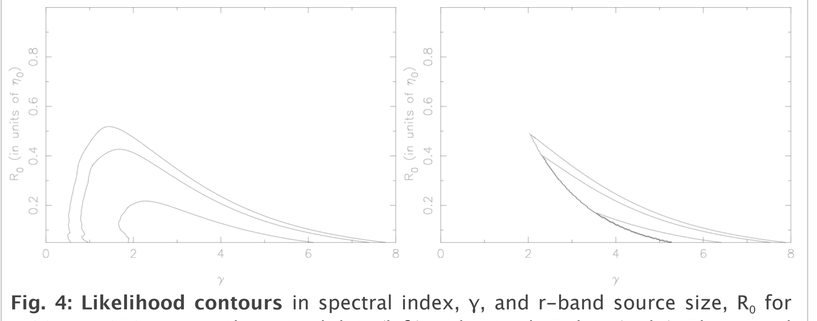

Fig. 4: Likelihood contours in spectral index, γ, and r-band source size, R_0 for MG0414+0534, using the optical data (left) and optical-IR data (right). The optical emission region is <0.5 Einstein radii (95%). Taken at face value, the IR data rules out a Shakura-Sunyaev disk (γ=1.3)

Conclusions

For MG0414+0534, we place an 95% upper limit on the innermost r-band emission region of $1.9\times10^{14}\,h_{70}^{-1/2}\,(M/M\odot)^{1/2}$ metres, or roughly 7 ($h_{70}^{-1/2}\,(M/M\odot)^{1/2}$) light days. We tentatively exclude a Shakura-Sunyaev disk (γ=1.3). Analysis of the data is still under way (Bate, Floyd & Webster, in preparation).

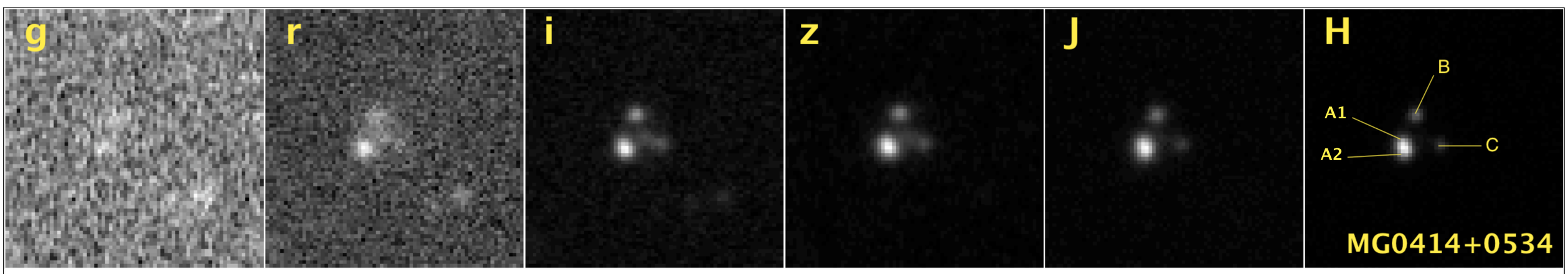

Fig. 2: Magellan IMACS + PANIC imaging of MG0414+0534 (November 2007). The anomalous flux ratio, A1/A2 increases as we move blueward.

References

B+07: Bate, Webster & Wyithe 2007, MNRAS, **381**, 1591
C02: Chiba, M. 2002, ApJ, 565, 17
C+07: Congdon, Keeton & Osmer, 2007, MNRAS, **376**, 434
DK02: Dalal, N., & Kochanek, C. S. 2002, ApJ, 572, 25
K+96: Kayser et al. 1986
L+95: Lawrence et al. 1995, AJ, **110**, 2570
MS98: Mao, S., & Schneider, P. 1998, MNRAS, 295, 587
MM01: Metcalf, R. B., & Madau, P. 2001, ApJ, 563, 9
SW02: Schechter & Wambsganss 2002, ApJ, **580**, 685
WMS95: Witt, Mao & Schechter 1995, ApJ, **443**, 18
W+90: Wambsganss et al. 1990
W+05: Wayth, O'Dowd & Webster 2005, MNRAS, **359**, 561